

IMPEDANCE EVALUATION OF PF IN-VACUUM UNDULATOR (IVU) WITH THEORIES AND SIMULATIONS AND EXPERIMENTAL CONFIRMATION OF THEM BY THE TUNE MEASUREMENT

O. Tanaka[†], N. Nakamura, T. Obina, and K. Tsuchiya, High Energy Accelerator Research Organization (KEK), Tsukuba, Japan

Abstract

Four In-Vacuum Undulators (IVU) were recently installed to Photon Factory (PF) at KEK. The estimate of their impedance and kick factors is a very important issue, because they could considerably increase the total impedance of PF. Moreover, the coupling impedance of the IVUs could lead to the beam energy loss, changes in the bunch shape, betatron tune shifts and, finally, to the various beam instabilities. Using the simulation tool (CST Particle Studio), longitudinal and transverse impedances of the IVUs were evaluated and compared to analytical formulas and measurement results. The study provides guidelines for mitigation of unwanted impedance, for an accurate estimate of its effects on the beam quality and beam instabilities and for the impedance budget of a newly designed next-generation machine which has many IVUs and small-aperture beam pipes.

INTRODUCTION

Accelerator components can interact with bunched particles through their inducing wake fields and impedance. Impedances lead to unwanted effects such as beam energy loss, changes in the bunch shape, betatron tune shifts, and to the various beam instabilities. Knowledge of impedances of the accelerator components is of a great importance because it allows to improve the performance the accelerator essentially. Therefore, they should be carefully estimated and evaluated in the very beginning of the design process of any high intensity machine.

At KEK Photon Factory (PF) light source, we have four newly installed In-Vacuum Undulators (IVUs). The IVU's vacuum chamber has a complex geometry. It consists of two taper transitions between the undulator and the beam chamber, one copper plate on the undulator magnets for RF shielding of the magnets from a beam, and two step transitions between the octagon and the taper region. Each part makes its own impact on the total frequency dependent impedance of the entire IVU. Design issues of IVU including taper regions, undulator plates and step transitions are well-studied (see, for example, [1 – 4]). Such Insertion Devices (IDs) are known to make small impacts on the total impedance of a machine [5]. However, the PF IVUs were installed much after the construction of the ring itself was completed, and there was a need of the proper IVU's impedance evaluations.

To quantify IVUs induced impedance we engaged both a powerful simulation tool (Wakefield Solver of CST Particle Studio [6]), and theoretical assessments (for

cross-checking the results of simulation), and, finally, an experimental reconciliation of the impedance values obtained from our studies. Such a comprehensive analysis shown in this article will be a standard procedure for the design of new accelerators. It allows to predict the thresholds of instabilities and to assess the influence of collective effects [7 – 8].

A few decades ago only 2D modeling of devices with axial symmetry was available. And to evaluate the impedances of real sections of the accelerator, scientists had to rely entirely on the results of the measurements [9]. Nowadays 3D impedance simulation tools (CST Particle Studio, GdfidL, MAFIA, etc.) have comparably good reliability and improved performance. Therefore, they provide an ability to simulate IDs and accelerator components with their full geometries. For example, at PETRAIII the wakefields of the whole IVU vacuum vessel were evaluated, although it required a considerable computing powers [2]. In the process of simulation of wakefields and impedances, the attention of scientists has been gradually shifted to the consideration of chamber shapes different from the circular geometry (rectangular, elliptical). Thus, we began to distinguish between dipolar (or driving) and quadrupolar (or detuning) contributions to the transverse impedance, whereas only impedance of the dipole mode has been studied previously. This new treatment gives an advantage to obtain different impedance effects on the beam dynamics. Namely, the dipolar wake provides an information about instabilities growth rate. And quadrupolar wake impacts on incoherent effects such as emittance growth and damping. This approach is a courtesy of CERN impedance group [10 – 11].

In this study we show how we identify the major impedance contributors and evaluate their impedance using theoretical formulas, CST Studio simulations and measurements. The KEK future light source will include one IVU for each lattice cell, therefore many IVUs are planned to be installed. Evaluation and improvement of their impedance is one more target of the present study. Now, let us discuss the details of these impedance evaluations, and its experimental confirmation.

IMPEDANCE EVALUATION FOR PF IVU BY SIMULATIONS AND THEORY

The PF IVU consists of three parts (see Fig. 1 a) – c)). Each of these parts impacts on the total impedance of the IVU. They are:

- Taper between the flange and the undulator (200 μm thick) for the geometrical impedance.

[†] olga@post.kek.jp

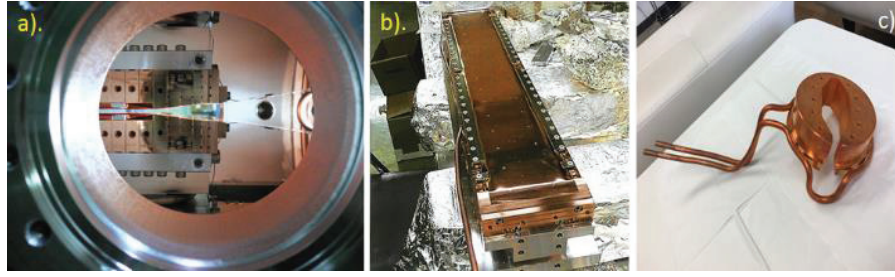


Figure 1: Three major impedance contributors of PF IVU: a). Taper between the flange and the undulator (200 μm thick) for the geometrical impedance; b). Copper plate (60 μm copper and 25 μm nickel coating) on top of the undulator for the resistive-wall impedance; c). Step transition from the octagon to the rectangular chambers.

- Copper plate (60 μm copper and 25 μm nickel coating) on top of the undulator for the resistive-wall impedance.
- Step transition from the octagon to the rectangular chambers.

In the following they will be treated separately.

Geometrical Impedance of Taper

To calculate the pure geometrical impedance of the taper, we first assume the perfectly conductive material instead of the copper resistivity. The CST model of the taper is shown in Fig. 2. It is known that a very fine mesh (Δz) is needed for accurate calculations of the taper impedance. The empirical formula [12]:

$$100 \leq \frac{a\phi}{\Delta z} \cdot \frac{\sigma_z}{\Delta z}. \quad (1)$$

Here a is a chamber radius, ϕ is a taper angle, and σ_z is the bunch length ($\sigma_z = 10\text{mm}$ in the PF case). For the PF IVU the mesh size is found to be $\Delta z \leq 150\mu\text{m}$.

The IVU impedance is greatly affected by the size of its gap ($2b$ in Fig. 2). When the ID is closed, even a difference of 0.5 mm in the gap yields a drastic increase of impedance. For a better and more economical design in future, we also studied the dependence of kick factors on the taper width. Conclusion before the results are: the present 100 mm is reasonable and close to optimal width. For the future IVU designs, the length of the taper (or its angle) is one of the key parameters of impedance evaluation. Its consideration was excluded from the present study because the IVUs were already designed and installed.

The taper structure is known to produce nearly pure inductive impedance even with a vessel included:

$$Z_l = -i\omega L, \quad W_{10}(z) = Lc \frac{d}{dz} \delta(z/c), \quad (2)$$

where Z_l is a longitudinal impedance of the taper, ω is a frequency, and L is the inductance. The theoretical formula for longitudinal impedance reads [13] (see Figs. 3 – 5):

$$\frac{Z_l}{n} = -i \frac{Z_0 \omega_0}{4\pi c} \int_{-\infty}^{\infty} (g')^2 F\left(\frac{g}{w}\right) dz, \quad (3)$$

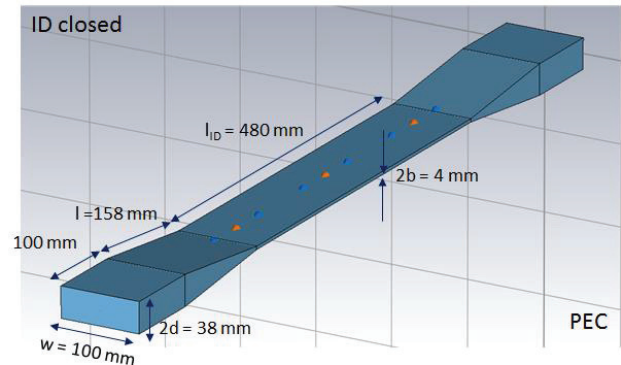


Figure 2: CST model of the IVU taper.

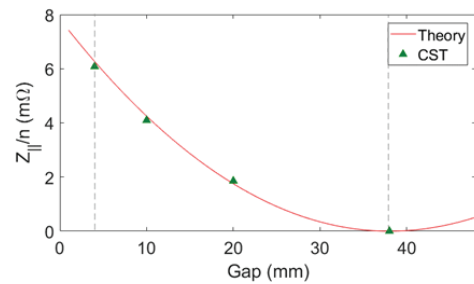


Figure 3: Normalized longitudinal impedance of the taper (gap dependence, width fixed to 100 mm) by theory (red line), and by simulations (green triangle).

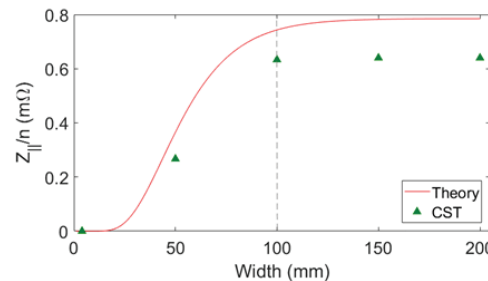


Figure 4: Normalized longitudinal impedance of the taper (width dependence, gap fixed to 50 mm) by theory (red line), and by simulations (green triangle).

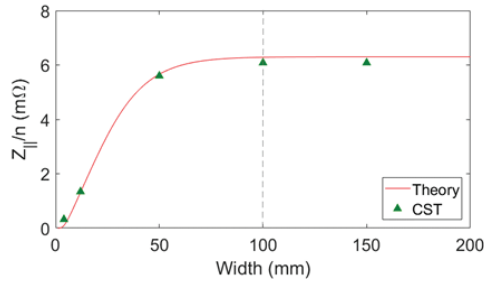


Figure 5: Normalized longitudinal impedance of the taper (width dependence, gap fixed to 4 mm) by theory (red line), and by simulations (green triangle).

$$F(x) = \sum_{m=0}^{\infty} \frac{1}{2m+1} \operatorname{sech}^2\left((2m+1)\frac{\pi x}{2}\right) \tanh\left((2m+1)\frac{\pi x}{2}\right). \quad (4)$$

Here $Z_{||}/n$ is the normalized longitudinal impedance, $Z_0 = 377\Omega$ is the impedance of the free space, and ω_0 is the angular revolution frequency. At PF $\omega_0 = 2\pi \cdot 1.6\text{MHz}$. The parameter g describes the vertical profile of the taper along the z axis, and w is the width of the taper ($b \leq w \leq l$).

We need a careful treatment of the transverse impedance, since it includes both the dipolar and the quadrupolar components [10]:

$$W_{y,tot}(y_1, y_2, z) = W_{y,dip}(z)y_1 + W_{y,quad}(z)y_2, \quad (5)$$

where $W_{y,tot}(y_1, y_2, z)$ is a total wake received by the beam. In CST simulations they can be calculated by displacing the beam and the wake integration path separately [11]. According to Krinsky [14], theoretical formula for dipolar impedance is as follows:

$$Z_{yD}(k) = -i \frac{Z_0}{2\pi b} \int_{-\infty}^{\infty} \frac{\xi^2}{\sinh^2 \xi} \sum_{n=0}^{\infty} \delta_n \frac{H(k_n, k) + H(k_n, -k)}{2ik_n b} d\xi \quad (6)$$

and

$$P(p, k) = \int_{-\infty}^{\infty} \int_{-\infty}^{\infty} S'(z_1)S'(z_2)e^{i(p+k)(z_1-z_2)} dz_1 dz_2, \quad (7)$$

where the width $w \rightarrow \infty$, the parameter k is a perturbation wave number, $k_n b = \sqrt{(kb)^2 - \xi^2 - (\pi n)^2}$. The function of the longitudinal position $S(z) = (a(z) - a_0)/a_0$ means a fractional deviation of the taper radius from the average one (a_0). For analytical estimation of the quadrupolar impedance, a formula derived by Stupakov [13] is used ($b \leq w \leq l$):

$$Z_{yQ} = -i \frac{\pi Z_0}{4} \int_{-\infty}^{\infty} \frac{(g')^2}{g^2} G\left(\frac{g}{w}\right) dz, \quad (8)$$

with

$$G(x) = x^2 \sum_{m=0}^{\infty} (2m+1) \times \operatorname{sech}^2\left((2m+1)\frac{\pi x}{2}\right) \tanh\left((2m+1)\frac{\pi x}{2}\right). \quad (9)$$

Both the dipolar and the quadrupolar impedances produce vertical kick factors. In the case of Gaussian beam their relation could be expressed by the following:

$$k_y = \frac{\operatorname{Im} Z_y c}{2\sqrt{\pi} \sigma_z}. \quad (10)$$

Figures 6 - 9 show the comparison of the analytical Eqs. (6) - (7) and (8) - (9) with the CST simulation results for the dipolar and quadrupolar vertical kick factors of the taper.

To sum up, the calculation of kick factors is most important since it provides additional coherent vertical tune shift. During machine measurements a tune shift could be detected. It includes both of dipolar and quadrupolar impacts.

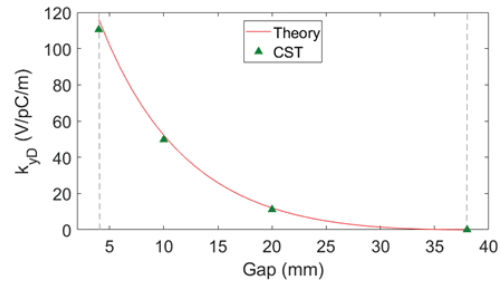


Figure 6: Dipolar vertical kick factor of the taper (gap dependence, width fixed to 100 mm) by theory (red line), and by simulations (green triangle).

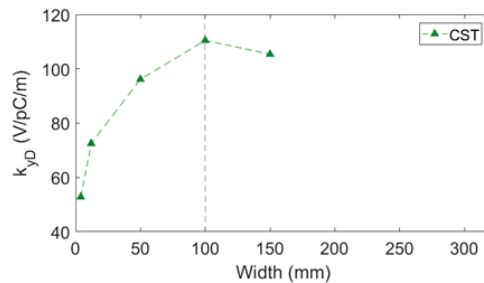
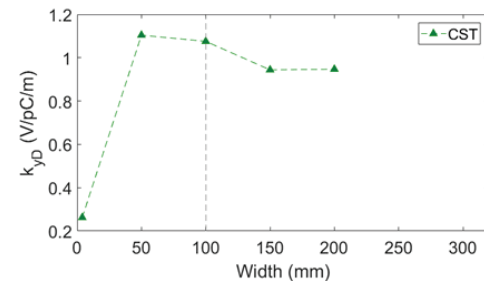


Figure 7: Dipolar vertical kick factor of the taper (width dependence) by simulations. The gap fixed to 50 mm (top), the gap fixed to 4 mm (bottom).

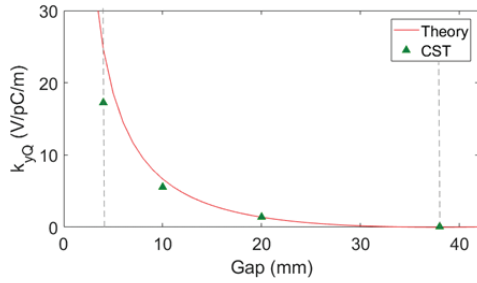


Figure 8: Quadrupolar vertical kick factor of the taper (gap dependence, width fixed to 100 mm) by theory (red line), and by simulations (green triangle).

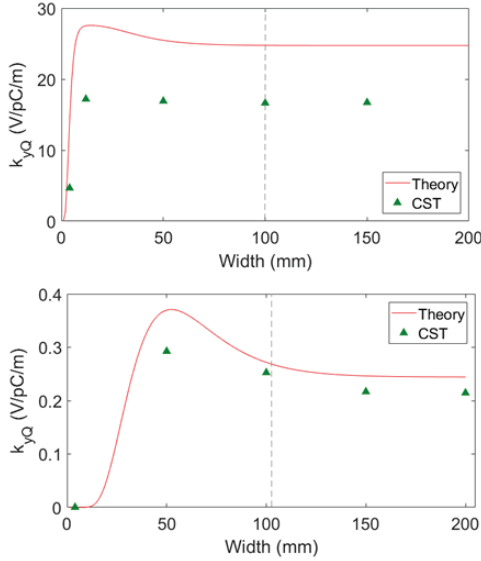


Figure 9: Quadrupolar vertical kick factor of the taper (width dependence, gap fixed to 4 mm (top), to 50 mm (bottom)) by theory (red line), and by simulations (green triangle).

Resistive-Wall Impedance of Undulator

By using the copper resistivity in CST, we can calculate the resistive-wall impedance of the undulator with the copper plate (the electric conductivity of copper is $\sigma_c = 5.9 \times 10^7 S/m$). The CST model of the undulator RF shielding with the Cu plate is shown in Fig. 10.

The vertical kick factor of the undulator plates was estimated using the following relation [15]:

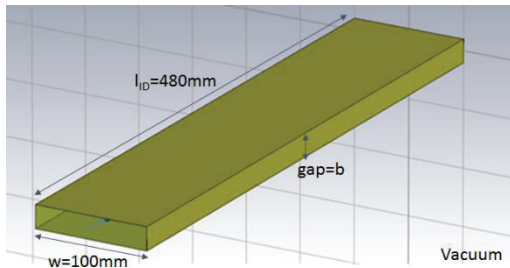


Figure 10: CST model of the undulator RF shielded by the copper sheet.

$$k_{yR.W.} = \frac{cL}{8b^3} \sqrt{\frac{2Z_0 c}{\sigma_c}} \Gamma\left(\frac{5}{4}\right), \quad (11)$$

where L is a length of the undulator ($L = 480\text{mm}$ for the PF IVU), and $\Gamma(5/4) = 0.9064$. The comparison between Eq. (10) and the CST simulation is given in Fig. 11. It demonstrates an excellent agreement between theory and simulations.

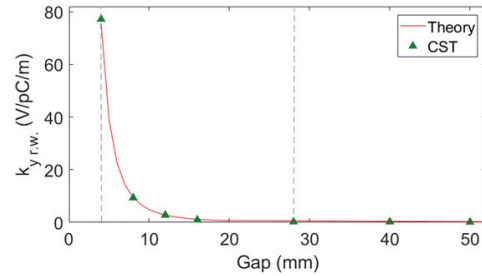


Figure 11: Resistive-wall vertical kick factor of the undulator (gap, dependence, width fixed to 100 mm, length fixed to 480 mm) by theory (red line), and by simulations (green triangle).

Geometrical Impedance of Step Transition

Low-frequency impedance of the step transition at the beginning of the taper was estimated using CST. Corresponding dipolar and quadrupolar kick factors have very small contributions to the total vertical kick factor and saturate at width $w = 150\text{mm}$. The impact of the step transition is three orders less than other components; therefore, we ignore it in the following treatment.

Total Transverse Impedance of the IVU

The total vertical kick factor due to 1 IVU including dipolar and quadrupolar kicks of the taper and resistive-wall kick of the undulator copper plates is summarized in Fig. 12. Table 1 provides more detailed information regarding the kick values.

An excellent agreement is seen between the theoretical predictions and the CST Studio simulations for PF IVU. Therefore, the new impedance evaluations of PF IVU are accurate enough in the framework of the theory and the simulation codes. We can use these calculation results and computation resources and techniques for future impedance measurements, for the design of new IVUs, and even for the impedance budget of the components of any new accelerator.

Before moving to the next section (tune shift measurement) some preparation work should be done. Namely, we need to evaluate an additional betatron tune shift ($\Delta\nu$) by 4 IVU at PF. We apply the well-known relation [16]:

$$\frac{\Delta\nu}{I_b} = -\frac{4\langle\beta k_y\rangle}{4\pi f_0(E/e)}, \quad (12)$$

Content from this work may be used under the terms of the CC BY 3.0 licence (© 2018). Any distribution of this work must maintain attribution to the author(s), title of the work, publisher, and DOI.

where I_b is the bunch current, $f_0 = 1.6\text{MHz}$ is a revolution frequency of PF ring, and E is the beam energy ($E = 2.5\text{GeV}$ at PF). With the kick data shown in Table 1, and average betatron function in the center of the taper $\beta_{y,taper} = 0.6406\text{ m}$, and in the center of the undulator $\beta_{y,RW} = 0.4657\text{ m}$, one can obtain the tune shift value per unit of current $\Delta\nu/I_b = -9.33 \times 10^{-6}\text{ mA}^{-1}$ as the simulation result, and $\Delta\nu/I_b = -9.967 \times 10^{-6}\text{ mA}^{-1}$ as the analytical result.

Table 1: Vertical Kick Factors of PF IVU

Vertical kick factor per 1 IVU		CST PS	Theory
Taper vertical kick factor, V/pC/m	Dipolar	110.47	116.13
Undulator vertical kick factor, V/pC/m	Quadrupolar	16.64	24.61
Undulator vertical kick factor, V/pC/m	Dipolar	50.80	75.57
Undulator vertical kick factor, V/pC/m	Quadrupolar	26.40	75.57
Total vertical kick factor, V/pC/m		204.31	216.31

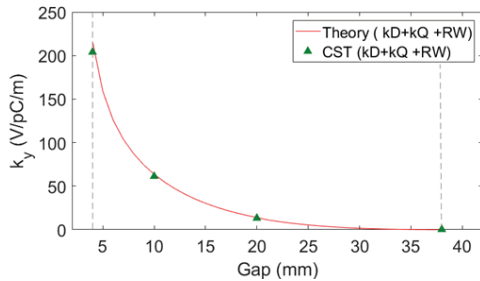


Figure 12: Total vertical kick factor of the IVU (gap dependence, width fixed to 100 mm) by theory (red line), and by simulations (green triangle).

MEASUREMENTS OF KICK FACTORS

We carried out tune shift measurements at PF based on the RF-KO (RF Knock Out) method [16]. In this method the responses of the strip line kicker oscillations were measured by sweeping the bunch current (equal to changing the betatron frequency) using a spectrum analyser equipped with a tracking generator. The switch to the single bunch operation mode and switch-off of the feedback system are crucial conditions for this measurement. In the multi-bunch mode, the current dependence of the tune shift is rather small. The feedback system introduces false signals and greatly influences the measurement result. Therefore, it is important to keep the bunch current below the instability threshold.

The additional tune shift corresponds to a difference of the vertical tune shifts for ID open (gap=38mm) and ID closed (gap=4mm) cases. We closed all four IVUs simultaneously to increase the effect. In fact, we tried to close the ID gaps one by one, and we do indicate reasonable tune shifts. One of the results of the tune shift measurement is shown in Fig. 13. The data were measured manually about 20 times at each current value with a step of 0.5~1 mA. We obtain the average tune shift of four meas-

urements to be $\Delta\nu/I_b = (-11.7615 \pm 1.4955) \times 10^{-6}\text{ mA}^{-1}$ (including the data fitting error).

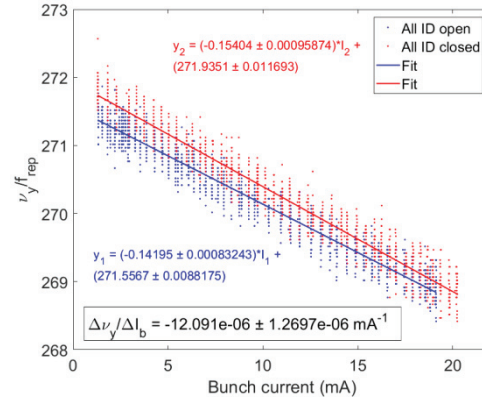


Figure 13: Tune shift measurement result.

An alternative method to measure the vertical kick factor of the IVU, called “the orbit bump” method, was introduced in [17] and further developed in works [18 – 19]. It creates an orbit bump at the location including IVU. One needs to measure the orbit deviations at many BPM positions to reduce statistical errors. In addition, there is a need to repeat the above procedure for different orbit bumps and bunch charges to eliminate systematic errors caused by intensity dependent behavior of BPM electronics. Finally, using the analytical formula and the Twiss parameters of the ring, we can identify the kick factor of IVU. The orbit bump (Y_0) creates orbit deviations proportional to the kick factor of IVU along the ring [1]:

$$\Delta y(s) = \frac{\Delta q}{E/e} k_{y,y_0} \frac{\sqrt{\beta(s)\beta(s_0)}}{2 \sin(\pi\nu)} \cos[\mu(s) - \mu(s_0) - \pi\nu], \quad (13)$$

Here Δq is a bunch charge variation, $\beta(s)$ is a betatron function, s_0 is an impedance location, and $\mu(s)$ is a betatron phase advance. The corresponding measurement is scheduled in this spring.

CONCLUSION

In summary, we have identified the major impedance contributors of PF IVU and successfully evaluated their impedance using theoretical formulas, CST Studio simulations and measurements. The three evaluations show very good agreements. The present methods and procedures will greatly help the design of future IVU for further reduction of impedance.

ACKNOWLEDGEMENT

We would like to thank the members of PF storage ring and operational staff for their help in achieving the necessary stable injection rate to demonstrate the tune shift caused by four IVU. Additional thanks to the monitor group for many useful advises in experimental setup.

REFERENCES

- [1] V. Smaluk *et al.*, “Coupling impedance of an in-vacuum undulator: Measurement, simulation, and analytical estimation.”, *Phys. Rev. ST Accel. Beams*, vol. 17, p. 074402, Jul. 2014.
- [2] E. Gjonaj *et al.*, “Computation of wakefields for an in-vacuum undulator at PETRA III”, in *Proc., 4th Int. Particle Accelerator Conf. (IPAC 2013)*, Shanghai, China, May, 2013, paper TUPWA008, pp. 1736-1738.
- [3] F. Cullinan *et al.*, “Evaluation of In-Vacuum Wiggler Wakefield Impedances for SOLEIL and MAX IV”, presented at the 22nd European Synchrotron Light Source Workshop (ESLS XXII), Grenoble, France, Nov. 2014. http://www.esrf.eu/files/live/sites/www/files/events/conferences/2014/XXII%20ESLS/CULLINAN_wigglerimpedance.pdf
- [4] T.F. Günzel, “Coherent and incoherent tune shifts deduced from impedance modelling in the ESRF-ring”, in *Proc., 9th .8.124403 European Particle Accelerator Conf. (EPAC 2004)*, Lucerne, Switzerland, July, 2004, paper WEPLT083, pp. 2044-2046.
- [5] T. Tanaka, “In-vacuum undulators”, in *Proc., 27th Int. Free Electron Laser Conf. (FEL2005)*, Palo Alto, USA, Aug. 2005, paper TUOC001, pp. 370-377.
- [6] CST-Computer Simulation Technology, CST PARTICLE STUDIO, <http://www.cst.com/Content/Products/PS/Overview.aspx>.
- [7] E. Belli *et al.*, arXiv:1609.03495.
- [8] K. Bane, “Review of collective effects in low emittance rings”, presented at the 2nd Topical Workshop on Instabilities, Impedance and Collective Effects (TWIICE2), Abingdon, UK, Feb. 2016. https://indico.cern.ch/event/459623/contributions/1131155/attachments/1224365/1791598/Bane_collective_1er.pdf
- [9] T. Hara *et al.*, “Spring-8 in-vacuum undulator beam test at the ESRF”, *Journal of Synchrotron Radiation*, vol. 5, part. 3, pp. 406-408, May. 1998.
- [10] B. Salvant, “Transverse single-bunch instabilities in the CERN SPS and LHC”, presented at the Beam Physics for FAIR Workshop, Bastenhaus, Germany, Jul. 2010. <https://indico.gsi.de/event/1031/>
- [11] C. Zannini, “Electromagnetic simulation of CERN accelerator components and experimental applications”, Ph.D. thesis, Phys. Dept., Ecole Polytechnique Fédérale de Lausanne, Lausanne, Switzerland, 2013.
- [12] O. Frasciello, “Wake fields and impedances of LHC collimators”, presented at the 100th National Congress of Italian Physical Society (SIF 2014), Piza, Italy, Sep. 2014.
- [13] G.V. Stupakov, *Phys. Rev. ST Accel. Beams* 10, 094401 (2007).
- [14] S. Krinsky, *Phys. Rev. ST Accel. Beams* 8, 124403 (2005).
- [15] A. Piwinski, “Impedance in lossy elliptical vacuum chambers”, DESY, Hamburg, Germany, Report No. DESY-94-068, Apr. 1994.
- [16] S. Sakanaka, T. Mitsuhashi, and T. Obina, *Phys. Rev. ST Accel. Beams* 8, 042801 (2005).
- [17] V. Kiselev and V. Smaluk, “Measurement of local impedance by an orbit bump method,” *Nucl. Instrum. Methods A* 525, 433 (2004).
- [18] L Emery, G. Decker, and J. Galayda, in *Proc., 19th Particle Accelerator Conference (PAC2001)*, Chicago, USA, Aug. 2001, paper TPPH070, pp. 1823-1825.
- [19] E. Karantzoulis, V. Smaluk, and L. Tosi, *Phys. Rev. ST Accel. Beams* 6, 030703 (2003).